Strength of Bolted Lap Joints in Steel Sheets with Small End Distance

Chu Ding[1], Shahabeddin Torabian[2], Benjamin W. Schafer[3]

[1] Graduate Research Assistant, Department of Civil and Systems Engineering, Johns Hopkins University, Baltimore, MD, United States
[2] Adjunct Associate Research Scientist, Department of Civil and Systems Engineering, Johns Hopkins University, Baltimore, MD, United States
[3] Professor, Department of Civil and Systems Engineering, Johns Hopkins University, Baltimore, MD, United States

Abstract

The objective of this work is to investigate the shear capacity of small end distance lap joints in sheet steel fastened with a single bolt. For bolted connections in shear, the current American Iron and Steel Institute (AISI) specification does not differentiate between tilting limit states, where the fastener rotates and thin sheet curls, and non-tilting limit states such as bearing and tearing. An experimental program consisting of 36 bolted specimens with small end distance, 18 subject to tilting, and 18 not subject to tilting, were conducted to explore this phenomenon. The conducted tests were compared to available predictions in AISI S100-2016 and the literature. The comparison indicates that tilting needs to be explicitly considered in the tested condition. Recommendations are provided for design. There is a need for future work to investigate multi-bolt configurations with small end distance and connections with members.

Introduction

The current design of cold-formed steel (CFS) bolted connections recognizes several potential failure modes for connected plates (Fig. 1): bearing, end tear-out, and net section fracture. The end tear-out failure mode, also known as shear rupture in the current AISI Specification (AISI S100 2016) or end pull-out in other specifications (e.g., AS/NZS 4600 2005), usually occurs under relatively small end distances. In a “pure” end tear-out failure, the connection deforms with the bolt tearing through the sheet in the loading direction, leaving two parallel shear paths and piling up steel in front of the bolt. Under this failure mode, the connection resistance is provided by the shearing capacity of the parallel shear paths; the connection fails when fracture forms along the paths. The fracture initiates from the bolt hole and propagates to the end of the sheet.

End tear-out was first studied by Winter (1956), in which end tear-out is classified as one of the three failure modes for connected plates of bolted cold-formed steel connections. Based on this work, the design equation of earlier editions of the AISI specification was developed, e.g. up to, AISI S100 (2007). End tear-out has been investigated in other studies including Zadanfarrokh and Bryan (1992) who studied small end distance bolted connections with curling restraint; Rogers and Hancock (1998) who studied end tear-out on bolted connections with high-strength steel and most recently Xing et al. (2020) who investigated small end distance bolted connections with thin cold-reduced sheets and proposed new design equations.

End tear-out, as the dominating failure mode under small end distance, is often excluded in previous experimental studies, as in general it is presumed that specifications will limit this failure mode by prescriptive criteria. As a result, bearing and net section fracture are more commonly studied. Teh and Uz (2015) performed a study of end tear-out failure in the context of hot-rolled steel and through a large collection of existing experimental data were able to provide novel design equations that improve the accuracy in predicting connection capacity. Teh and Uz (2015) demonstrated that the use of the gross shear plane area often leads to overestimation of strength while using the net shear plane area can be quite conservative. Accordingly, an alternate equation, based on “active planes”, was proposed and was found to be capable of producing consistently accurate predictions. However, as a study focused on thicker specimens, the effect of tilting, a phenomenon that often coincides with thin steel sheet, is not investigated in Teh and Uz (2015). Titling, as shown in Fig. 2(a), is a unique feature of thin sheet connections which is not observed in thick plate connections, as depicted in Fig. 2(b). The concept of tilting is further detailed subsequent to additional discussion on end tear-out.

Rogers and Hancock (1998) conducted a series of bolted connection tests fabricated from low ductility high-strength (G550) cold-formed steel sheets. This study found that the end tear-out design equations in AS/NZS 4600 (2005) and AISI Specification (1996) to be unconservative. They further found that the strength had to be reduced by 0.75 in connection limit states to find good agreement with their tests. This led to the adoption of a reduction factor for low ductility G550 sheet steels in later editions of the AS/NZS 4600 and AISI S100 standards.

In the 2012 AISI Specification (AISI S100 2012) as part of a North American harmonization effort, AISI's longstanding empirical end tear-out design equation was abandoned in favor of a more mechanically motivated Canadian expression. In the new expression, based on hot-rolled steel block shear research (Kulak and Grondin 2001) the resistance is predicted based on the shearing strength of two pre-defined shear paths with lengths equal to the net end distance. This series of changes prompted interest in a systematic assessment of currently available design equations for end tear-out failure.

Lap shear connections in thin screw-fastened sheets have long been observed to suffer from tilting. Lap shear connections in thin bolted sheets also may suffer from this limit state. As shown in Fig. 2(a), tilting is initiated by the small eccentricity in the connection and the minimal rigidity of the thin plate, and includes fastener rotation and sheet curling. Tilting is much reduced in thicker plates (Fig. 2 (b)), largely due to the fact that the plate bending rigidity increases proportionally to the plate thickness cubed. For thin sheet steel connections tilting has been recorded in the literature (Carril et al. 1994; Chong and Matlock 1975; Fox and Schuster 2006; Rogers and Hancock 2000). The existence of tilting often complicates the pre-defined limit state definitions, particularly when they are borrowed directly from hot-rolled steel, sometimes causing misinterpretation of limit states. For bearing failure, it was found that plate curling/tilting induces additional through-thickness shear stress (Rogers and Hancock 2000). The final fracture limit state induced from tilting is two tearing paths originating from the hole to end of plate, resembling net section failure. This has led to some interpretations of this bearing failure as net section failure. Regarding the influence of tilting on connection strength, related numerical research on bolted stainless steel connections has shown up to a 25% strength reduction connection failure capacity due to tilting in net section or block shear failure (Soo Kim and Kuwamura 2007). In the current literature and CFS specifications, the effect of tilting is not directly addressed for bolted connections and thus needs further study. The study herein attempts to answer these basic bolted connection issues by conducting a limited experimental program consisting of both single-lap and double-lap bolted connection tests.

Available Design Equations

For a lap joint with a single bolt and geometry as shown in Fig. 3, there are a variety of strength design expressions available in national specifications, and in the literature. This section introduces the most prominent design methods in current use. A summary of all the design equations discussed in this section can be found in Table 1.

AISI S100-2007 end tear-out equation

In the 2007 edition of the AISI Specification (AISI S100-2007), the shear rupture design equation (E3.1) is specified as

$$P_n = teF_u \tag{1}$$

where t is the plate thickness, e is the end distance from the center of the hole, and F_u is the ultimate strength of the plate. This design equation is based on the relation between bearing stress σ_b and e/d ratio revealed from test data (Yu 1982), where d is the bolt diameter. For small e/d ratio, it is found that $\sigma_b/F_u = e/d$. The equation $P_n = teF_u$ is obtained by substituting $\sigma_b = P_u/td$ into the previous relation. This equation was also adopted in Australian/New Zealand code for end tear-out strength (AS/NZS 4600 2005).

AISI S100-2012/2016 end tear-out equation

In the 2012 and 2016 edition of the AISI Specification (AISI S100-2012, 2016), the shear rupture design equation was updated. The new shear rupture design equation also appeared in the 2007 edition of the AISI Specification. However, in the 2007 edition, it was only used specifically for beam-end type bolted connection, not for general bolted connections. The shear rupture design equation for a lap joint with a single bolt is provided in 2016 as

$$P_n = 1.2te_{net}F_u \tag{2}$$

where e_{net} is the clear distance from the hole to the end. The ultimate shear stress at failure is approximated as $0.6F_u$ and two shear planes exist. The factor of 0.6 is a widely established shear coefficient, and is also supported by the experimental study conducted by Fox and Schuster (2006), in which the factor 0.6 is back-calculated from $\sigma_b/F_u = P_u/2etF_u$. It is worth noting that gross end distance e instead of net end distance e_{net} is used in this calculation. The AISI S100-

2012/2016 end tear-out equation is the same as the tear-out equations in the current and past edition of AISC (American Institute of Steel Construction) Specification (AISC 360 2010, 2016), when hole deformation at service load is a concern. When hole deformation is not a concern, the shear coefficient of 0.75 is used in the AISC specification instead. There is a subtle difference between the current and past AISC specifications: the current AISC Specification (AISC 360 2016) treats bearing and tear-out as separate limit states, while in the past edition (AISC 360 2010) tear-out is treated as a bearing limit state, although the design equations are the same.

Teh and Uz (2015) end tear-out equation

A modification of Eq. (2) has been proposed by Teh and Uz (2015). Instead of using the net end distance, the proposed equation adopts a shear path with length, L_{av}, being the average of gross end distance and net end distance, where $L_{av} = e_{net} + d_h/4$, resulting in:

$$P_n = 1.2(e_{net} + d_h/4)tF_u \tag{3}$$

Xing et al. (2020) end tear-out equation

A end tear-out equation has been recently proposed specifically for cold-reduced thin sheets by Xing et al. (2020). The prediction is modified from Teh and Uz (2015) and adds an additional factor, $(3d/e)^{1/5}$, which is used to account for catenary action of the material strip in the front of bolt hole resulting in the following expression:

$$P_n = 1.2(3d/e)^{1/5}(e_{net} + d_h/4)tF_u \tag{4}$$

Eurocode ECS (2006) end tear-out equation

Eurocode provides a related but slightly different methodology in EN-1993-1-3: 2006 (ECS 2006). Eurocode does not directly consider end tear-out as a separate failure mode; instead, the end tear-out limit state is considered through the bearing design equation. The initial form looks rather different from Eq. (1), but investigation reveals that it is essentially the same. The Eurocode equation for nominal strength is,

$$P_n = 2.5\alpha_b k_t F_u dt \tag{5a}$$

where $\alpha_b = \min(1.0, e/3d)$ and $k_t = (0.8t + 1.5)/2.5$ for 0.75 mm $\leq t \leq 1.25$ mm, $k_t = 1.0$ for $t > 1.25$ mm. The usage of the factor α_b is responsible for transitioning the equation between the basic form used for typical bearing failure, dtF_u, and the one for end tear-out failure, teF_u. For the type of small end distance ratio where end tear-out failure dominates, $\alpha_b = e/3d$. Eq. (5a) can be simplified to,

$$P_n = \begin{cases} (0.8t/3 + 0.5)teF_u & t \leq 1.25 \text{ mm} \\ teF_u/1.2 & t > 1.25 \text{ mm} \end{cases} \tag{5b}$$

AISI S100-2016 screwed connection tilting/bearing equation

A unique characteristic of thin plate cold-formed steel lap shear connections is the existence of tilting. Tilting is only considered in screwed connection design by the AISI specification (AISI S100 2016) – Section J4.3.1 specifies the strength as follows:

$$P_n = 4.2(t_2^3 d)^{1/2} F_{u2} \tag{6}$$

where t_2 and F_{u2} correspond, respectively, to the thickness and strength of the plate not in contact with the screw head. It is worth noting that this equation only applies when t_2 is smaller than t_1, the thickness of the plate in contact with screw head.

AISI S100-2016 bolted connection bearing equation

In AISI S100-2016, there is no explicit equation for bolted connection failure modes involving tilting. Instead, for the bearing design equation, a modification factor m_f is included to implicitly consider tilting. For example, m_f is equal to 1.33 for a non-tilting case (i.e., inside sheet of a double-lap configuration), while m_f is equal to 0.75 for one of the tilting cases (i.e., outside sheet of a double-lap configuration).

$$P_n = Cm_f dtF_u \tag{7}$$

where C is bearing factor dependent on d/t ratio.

Teh and Uz (2017) tilting/bearing equation

Teh and Uz (2017) investigated single-bolted lap joints with large end distance (e/d > 3) which failed in a tilting-bearing mode. A tilting-bearing design equation was proposed, which considers a power contribution for sheet thickness and sheet width.

$$P_n = 2.65d^{1/2}t^{4/3}w_{net}^{1/6}F_u \tag{8}$$

where w_{net} is the net sheet width, i.e. the sheet width minus the hole diameter.

Testing Program and Test Set-up

A test program on bolted connections in shear has been carried out at Johns Hopkins University in the Thin-Walled Structures Lab. The tests consisted of single-lap and double-lap shear configurations as shown in the uniaxial testing rig, Fig. 4, and in the schematic of Fig. 5. In total, 36 bolted connections were tested, including 18 single-lap shear connections and 18 double-lap connections. Each single-lap connection is matched with a double-lap connection of the same nominal geometry.

In these tests, beyond connection type, three other parameters were varied: hole diameter, sheet thickness, and the ratio of end distance to hole diameter. Two bolt diameters were selected: 7.9 mm (5/16 in) and 11.1 mm (7/16 in). The bolts were placed in oversized holes. Per AISI S100 (2016), for bolt diameter equal or smaller than 12.7 mm (1/2 in.), bolt holes 1.6 mm (1/16 in.)

larger than the bolt diameter are classified as oversized. Two oversized bolt holes, 9.5 mm (3/8 in.) and 12.7 mm (1/2 in.), were used in the tests. In common cold-formed steel industry practice, washers are rarely installed unless uniquely specified by the design engineer; therefore, no washers were installed for the specimens. The majority of the bolts were installed loosely to mitigate friction between the sheets. For eight test specimens in the first phase of testing, bolts were installed snug tight by a wrench to a torque of 16.9 N-m (12.5 lbf-ft). These specimens are 12g-1/2-1.75dh-S, 12g-1/2-1.75dh-ID, 12g-3/8-1.50dh-S, 12g-1/2-1.50dh-S, 16g-1/2-1.50dh-ID, 12g-3/8-1.25dh-ID, 16g-1/2-1.25dh-S, 16g-1/2-1.25dh-ID. For later discussion, these specimens are labeled with an asterisk for clarity. The bolts used in the testing were all hex-head SAE Grade 8 bolts, with a minimum tensile strength of 1034 MPa (150 ksi), thus excluding the possibility of bolt shear.

Since the failure mode of interest is connection end tear-out, it was essential to choose connection configurations which eliminated unwanted failure modes. To eliminate bearing failure, a small ratio of end distance to hole diameter (e/d_h) was selected; specifically: 1.75, 1.50 and 1.25. It is worth noting that in this paper end distance ratio is defined as end distance, e, to hole diameter, d_h. To avoid net section tension failure, the sheet width is set at 38 mm (1.5 in.) for the 9.5 mm (3/8 in.) hole diameter as shown in Fig. 6 (a) and 50 mm (2.0 in.) for the 12.7 mm (1/2 in.) hole diameter as shown in Fig. 6 (b).

The sheet material for the specimens with 0.84 mm (33 mil, 20 ga.) and 1.37 mm (54 mil, 16 ga.) thickness were fabricated from cold-formed steel coils. The specimen with 2.46 mm (97 mil, 12 ga.) thickness was cut from the web of commercial cold-formed steel studs. The width of all the specimens were milled to the desired dimension with a tolerance of 0.05 mm (0.002 in) to ensure consistent width and avoid unwanted fracture. Mild steel was used throughout, with mechanical properties as shown in Table 2 found by testing of coupons in accordance with ASTM E8 (ASTM 2016). The longitudinal material properties were used in all the calculations.

All bolted specimens were tested in a 440 kN (100 kip) MTS two post universal testing machine (Fig. 4) with a 220 kN (50 kip) load cell with an accuracy of +/-20 N (4.5 lbf). The specimens were secured at each end by mechanical grips. For single-lap connections, to overcome the slight eccentricity induced in the testing rig, a 50 mm × 50 mm (2 in. × 2 in.) steel packing plate with the same thickness as the specimen was installed at each end to eliminate eccentricity (Fig. 5).

Two-dimensional digital image correlation (DIC) techniques were applied in the testing program to generate the strain field of the specimen under load. Before testing, the specimens were painted with a white coating and a layer of black speckles were created over the white coating. During the experiments, a camera, mounted in front of specimens, took pictures throughout the process. The pictures collected by the camera were fed into Ncorr (Blaber et al. 2015), an open-source DIC software, to perform the strain analysis.

Test Results and Observations

Failure observation

All specimens failed by fracture initiating from the front of the bolt holes. The failures discussed in this section refer to the complete and final fracture of the specimens. This occurs when a specimen completely loses its load-bearing capacity. The failure modes of the single-lap and double-lap connections share the same basic characteristics in that noticeable shear planes are observed at both sides of the bolt hole. However, sheets in the double-lap connection remain in-plane, Fig. 7 (a), while in the single-lap connections the sheets experience significant tilting as shown in Fig. 7 (b).

For double-lap connections, the connection plate remained in-plane until the final fracture. Two shear planes develop from each side of the deformed bolt hole. The shear planes develop at a slight angle to the longitudinal direction (Fig. 7 (a)). Additionally, the shear planes do not initiate at the net end distance, e_{net}, nor whole end distance, e. Instead, consistent with the observations by Teh and Uz (2015), the beginning of the shear path is located between the hole end distance, e, and net end distance, e_{net}.

In the case of single-lap connections, the eventual fracture is a mixture of end tear-out and tilting. Tilting is observed to initiate shortly after testing begins and the degree of tilting consistently increases until the final fracture. At final fracture, significant fastener rotation and sheet curling are observed as shown for a typical failure in Fig. 7(b). The out-of-plane deformation induces additional through-thickness tearing, as opposed to exclusively in-plane tearing as seen in the double-lap connections. Also, unlike the double-lap connections whose shear planes are almost parallel to each other, the shear planes in the single-lap connections are oriented at a larger angle to one another. In addition, the single-lap connections do not display the behavior of sheet piling in the front of the bolt holes, which is typical in double-lap connections.

Strength Reduction Due to Tilting

The ultimate capacity of each connection specimen is provided in Table 3. The single-lap and double-lap connections experience distinct limit states, with the double-lap failing in the classic end tear-out mode while the single-lap fails in a mixture of end tear-out and tilting. In terms of classical modes of fracture, it can be observed that the double-lap connections are driven by in-plane shear (mode II), while the single-lap connections, due to the tilting, are a combination of in-plane shear (mode II) and out-of-plane shear (mode III). Comparing the ultimate load of the single and double-lap condition, as provided in Table 3, gives a measure of the impact of the tilting on the strength.

Per Table 3 the single-lap connection strength is lower than its double-lap counterpart; except for thicker sheet (12 or 16 gauge) with small end distance ($1.25d_h$). These results indicate that a tilting-induced strength reduction for bolted connections should be considered. Based on the observation of Table 3, the extent of the tilting-induced strength reduction is stronger for specimens with thinner sheets or larger end distances. This result is reasonable, since the connections with thinner sheets are more susceptible to tilting, and the connections with larger end distance are less susceptible to end tear-out. Detailed examination of observed failure modes and the participation of the possible deformations are explored in the next section via the connection strain distribution determined from DIC analysis.

Load-deformation history and strain distribution

The load-deformation history of the tested connections is provided in Fig. 8. Deformation in Fig. 8 is the actuator displacement and thus includes unwanted contributions from sheet elongation as well as grip slippage, but since strength is the primary focus of this work, the data was found to be sufficient for globally studying the limit states.

In comparison to the double-lap connections, the single-lap connections experience more deformation at the ultimate capacity and eventual fracture. The larger deformation is attributed to the tilting.

DIC is applied to this testing program as a tool to explore the behavior of the bolted connections. Through analysis of the collected images, the von Mises strain evolution in the bolted connections until the conclusion of testing can be obtained. As provided in Fig. 9, the von Mises strain contours of the lower connected sheets at various stages of loading are shown. These stages include 50% of the ultimate load, 100% of the ultimate load, and 20% of strength degradation. With the aid of the pin hole loaded stress concentration chart (Schijve 2009) and assumption of elastic material, the maximum strain at the front of the bolt hole can be estimated at 25% of the ultimate load and 50% of the ultimate load. At the 25% of the ultimate load, the estimated maximum strain is 0.0014 while the DIC strain is 0.0020. At the 50% of the ultimate load, the estimated maximum strain is 0.0029 while the DIC strain is 0.0032. At both these load levels, the DIC strains are in reasonable agreement with expectation providing confidence in the observed DIC strain distribution.

Focusing on peak strength, the single-lap von Mises strain distributions for the tested specimens as developed from DIC are provided in Fig. 11 (a) and (b). The spatial distributions of the von Mises strain are similar among all the tested single-lap connections. The high-strain region originates from the end of the hole in bearing with the bolt shaft and expands towards the end of the connected plate. Transversely, the strain quickly dissipates once beyond the hole. One interesting finding is the existence of a small low-strain area right in front of the hole. Most, though not all the specimens, exhibit this strain feature at peak load. The existence of the small low-strain area leaves the remaining high-strain area shaped as two shear planes, confirming the tearing failure mode in the DIC observations.

The strain distributions from DIC provide an opportunity to examine the participation of end tear-out and tilting in the combined failure mode. The perspective that single-lap connection failure mode is a combined mode of end tear-out and tilting can be supported by the strain distribution obtained from DIC. In Fig. 11 (a), a comparison of the strain distributions at a section cut near the bolt hole is made between three specimens with the same geometry but varying in thickness. Each strain distribution is normalized to the maximum strain of the specimen. As shown in Fig. 11(a), the two thinnest specimens (which fail in tilting) are similar and characteristically different from the thickest specimen, which fails without significant tilting. A similar comparison of the strain distribution is provided as end distance is varied among the thinnest (20 g) specimens in Fig. 11 (b). As shown in Fig. 11(b), at the smallest end distance the observed strain at peak is influenced by end tear-out but less by the tilting observed in the larger end distance tests. Overall, the failure form of the single-lap connections is a combined response composed of (a) local response – end tear-out, and (b) global response – tilting, and the degree of participation depends on specimen geometry.

Comparison of Design Strength Predictions

General

In this section, the ultimate loads of the tested specimens are compared against predictions by the design equations previously summarized in Table 1. Comparison is conducted for each specimen and summarized in Table 4 (see Table A-1 in Appendix A for the test-to-predicted ratio of individual specimens). The design equations intended for tilting: AISI S100 J4.3.1 (2016) (Eq. (6)), AISI S100 J.3.1 (2016) (Eq. (7)) and Teh and Uz (2017) (Eq. (8)) are applied only to the single-lap specimens.

The summary statistics and reliability factors are summarized in Table 4. For the double-lap connections, test results from other researchers (He and Wang 2011; Xing et al. 2020) are also included in the data pool for analysis. The summary of the test-to-predicted ratios of each dataset is shown in Table 5. It is worth noting that the specimens in this paper are made from mild steel sheets with similar longitudinal and transverse properties (see Table 2), while the specimens by Xing et al. (2020) are cold-reduced sheets with important differences in material properties between longitudinal and transverse directions which must be considered.

For application to all specimens (single-lap and double-lap), there are two design equations that maintain overall average conservatism: the 2016 AISI end tear-out equation, and the Eurocode equation. Though underestimating strength for both single-lap and double-lap specimens, the 2016 AISI end tear-out equation is more conservative for double-lap (1.339) than single-lap (1.118). The Eurocode equation also underestimates the strength of both the single-lap (1.098) and the double-lap specimens (1.295). The 2007 AISI end tear-out equation along with Teh and Uz (2015) equation are found to be unconservative for single-lap specimen, with the test-to-predicted ratio of 0.877 and 0.883 respectively, although these two equations' prediction for double-lap specimen are in good agreement with test data (1.071 and 1.067 respectively). The newly proposed Xing et al. (2020) equation's predictions agree well with the double-lap connections but overestimate the strength of the single-lap connections. Overall, for double-lap connections, the 2007 AISI end tear-out equation, Teh and Uz (2015) equation and Xing et al. (2020) equation all agree with test data with reasonable accuracy. These three design equations share similar equation form and their differences in prediction are nonsignificant which are dependent on equation parameter tuning. Therefore, the 2007 AISI end tear-out equation, Teh and Uz (2015) equation and Xing et al. (2020) equation are all recommended for application to double-lap connections.

As for design equations only applied to single-lap specimens, it is interesting to find that the AISI bearing equation is significantly unconservative (0.791), further indicating that single-lap specimen failure is different from the classic bearing failure. Both the AISI screw titling/bearing equation and Teh and Uz (2017) equation are unconservative with respect to the test results. This shows that the AISI screw tilting/bearing equation cannot be directly applied to bolted connection. Also, it is worth noting that Teh and Uz (2017) equation was initially developed from connection tests with large end distances instead of small end distances discussed in this paper.

Recommended design equations

Based on the study in the previous sections, it is found that the current 2016 AISI end tear-out equation does not fit the available data well for specific configurations, either being unconservative or overly conservative, while the 2007 AISI end tear-out equation and the AISI tilting/bearing equation each have its advantage in their most applicable conditions. Therefore, it is recommended to simply take the minimum between the 2007 AISI end tear-out and the AISI tilting/bearing equation (i.e., Eq. (1) and (5)):

$$P_n = \min\left(4.2(t_2^3 d)^{1/2} F_{u2}, 1.2 t e_{net} F_u\right) \tag{9}$$

As Teh and Uz (2015) has slightly superior performance over the 2007 AISI end tear-out equation, it is also recommended that the minimum may be taken between Teh and Uz (2015) equation and the AISI tilting/bearing equation (i.e., Eq. (3) and (5)).

$$P_n = \min(4.2(t_2^3 d)^{1/2} F_{u2}, 1.2(e_{net} + d_h/4) t F_u) \tag{10}$$

As shown in Table 4, both of the recommend equations provide reliable strength prediction, with the mean test-to-predict ratio equal to 0.994 and 1.002 respectively.

Sheet thickness

This section explores the design equations under different sheet thickness configurations for the single-lap connections. As shown in Fig. 12, the design equations ignoring tilting, e.g., Eq. (1), (2), (3), (4), (5), are less conservative at smaller sheet thickness. On the other hand, the design equations considering tilting are more conservative for thinner sheets but less conservative for thicker sheets, e.g., Eq. (6), (7), (8). The recommended procedures: Eq. (9) and (10), take advantage of the two opposing trends to provide better strength prediction.

End distance

This section explores the design equations under different end distance ratios for single-lap connections. The design equations can be divided into two groups, those developed for end tear-out - Eq. (1), (2), (3), (4), (5), (9), (10), and those for bearing - Eq. (6), (7), (8). As shown in Fig. 13, the design equations focusing on end tear-out are found to be more conservative at smaller end distance ratios and less conservative at larger end distance ratios, which is the opposite for the design equations developed for bearing. Similarly, taking advantage of these two opposing trends, the recommended equations can achieve a more accurate strength prediction.

Reliability of Recommended Equation

Reliability of the recommended equations is studied in this section so that the resistance factor ϕ and safety factor Ω can be calibrated. The basic procedure in Section K2.1 of AISI S100-2016 is followed. According to the reliability procedure employed in AISI S100-2016, the resistance factor ϕ for LRFD design may be calculated as follows:

$$\phi = C_\phi (M_m F_m P_m) e^{-\beta_0 \sqrt{V_M^2 + V_F^2 + V_P^2 + V_Q^2}} \tag{11}$$

In Eq. (11), the calibration efficient C_ϕ is equal to 1.52 and V_Q is equal to 0.21 for LRFD (Meimand and Schafer 2014). The target reliability index β_0 is taken as 3.5 for connections per AISI S100 (2016). As for the other statistical parameters, the values of P_m and V_P for the recommended method 1 and 2 have been determined in the previous section respectively as (0.994, 0.108) and (1.002, 0.119) for single-lap specimen. The remaining statistical parameters from AISI S100-2016 include M_m = 1.10, V_M = 0.08, F_m = 1.00, and V_F = 0.05.

The results are provided in Table 4 and the resistance factor ϕ is determined to be 0.683 for recommend method 1 and 0.676 for recommend method 2. Both of the ϕ factors are rounded to 0.68 as reported in Table 4. Accordingly, the ASD safety factor is 2.34 for recommended method 1 and 2.37 for recommended method 2. Per editorial practice in AISI S100 ϕ may be rounded up to the nearest 0.05, i.e. 0.70, or perhaps for simplicity left the same as shear rupture, which is equal to 0.65.

Discussion

The single-lap connection differs from the double-lap connection due to the existence of tilting. The difference is reflected in observed limit states, ultimate load, and strain fields. The tilting introduces through-thickness tearing in the out-of-plane direction, perpendicular to the sheet plane. The additional shear is resisted by the sheet thickness. Different from in-plane tearing, the out-of-plane tearing is concentrated at the region of sheet separation, specifically the intercept of the sheet already torn and the remaining sheet to be torn. The authors hypothesize that the out-of-plane tearing is weaker than the in-plane tearing in both stiffness and strength. It would be worthwhile to investigate if such a difference exists. Meanwhile, the degree of in-plane bending may also affect behaviors. Conceptually, as the tilting angle increases, the out-of-plane tearing direction becomes more aligned with the thickness direction as opposed to being skewed, which should lead to lower tearing resistance. Knowledge of titling angle influence can improve understanding of the strength reduction by tilting. It is also worth noting that the degree of tilting decreases in multi-bolt configurations, in connections to sections, and potentially with other details such as large washers. Additional study on these configurations and greater clarity on under exactly what circumstances the tilting condition must be considered in design is needed.

In Table 3, the single-lap specimens at 1.25 end distance ratio with medium or high thickness are shown to achieve strength equal to or slightly higher than their double-lap counterparts. The tilting/curling effect in single-lap tests is reduced in specimens with small end distance and high thickness configurations, Thus, the strength in single-lap specimens is similar to double-lap specimens for those conditions. In addition, the authors hypothesize that the presence of the bolt head and nut bearing during tilting modestly widens the edge tear out failure path potentially leading to greater strength than in the double-lap condition where this does not occur. As shown in Fig. 8, the load-deformation curves of single-lap specimens are occasionally accompanied with sudden drops in load, e.g. 12g-3/8-1.50dh-S. The author hypothesizes that this phenomenon is caused by bolt thread slipping over the hole edge as bolt rotates.

Conclusion

Tests on small end distance bolted lap joints have shown that tilting reduces the shear capacity of the joints, indicating a need to explicitly incorporate the effect of tilting in current design equations for bolted cold-formed steel connections. This paper recommends using the minimum of two existing design equations: one for tilting/bearing and one for end tear-out, and shows that this provides reliable strength prediction against the conducted testing. For double-lap connections, this paper finds that several design equations provide acceptable reliability including the end tear-out equation in AISI S100 (2007), as well as expressions developed by Teh and Uz (2015), and Xing et al. (2020). Given that current industry practice often employs minimal end distance in connection design, it is important to ensure accuracy of the equations so that safety is assured as economy is pursued. The tests also highlight the uniqueness of cold-formed steel design in which local sheet bending can influence connection strength, as opposed to hot-rolled steel for which such effects are safely ignored. This paper does not address tilting from a fundamental mechanics standpoint. However, establishing the fundamental means that tilting alters lap-joint behavior is worth pursuing as future study, as are practical methods to limit tilting in bolted connections.

Data Availability Statement

Some or all data, models, or code that support the findings of this study are available from the corresponding author upon reasonable request, which include raw data points of tensile coupon tests, raw data points of connection tests and all images used for DIC analysis.

Acknowledgments

This paper is based on the work supported by American Institute of Steel and Iron (AISI) Small Fellowship Program - 1208430017. The authors are also grateful for the discussion with Prof. Lip Teh (University of Wollongong Australia) about the connection tests during his visit at Johns Hopkins University.

References

AISC 360. 2010. *Specification for Structural Steel Buildings*. AISC 360-10, American Institute of Steel Construction, Chicago, Illinois.

AISC 360. 2016. *Specification for Structural Steel Buildings*. AISC 360-16, American Institute of Steel Construction, Chicago, Illinois.

AISI. 1996. *North American Specification for the Design of Cold-Formed Steel Structural Members*. AISI, American Iron and Steel Institute, Washington, DC.

AISI S100. 2007. *North American Specification for the Design of Cold-Formed Steel Structural Members*. AISI S100-07, American Iron and Steel Institute, Washington, DC.

AISI S100. 2012. *North American Specification for the Design of Cold-Formed Steel Structural Members*. AISI S100-12, American Iron and Steel Institute, Washington, DC.

AISI S100. 2016. *North American Specification for the Design of Cold-Formed Steel Structural Members*. AISI S100-16, American Iron and Steel Institute, Washington, DC.

AS/NZS 4600. 2005. *Cold-formed steel structures.* Standards Australia ; Standards New Zealand, Sydney, N.S.W.; Wellington [N.Z.

ASTM E8/E8M. 2016. *Test Methods for Tension Testing of Metallic Materials*. ASTM International. https://doi.org/10.1520/E0008_E0008M-16A.

Blaber, J., Adair, B., and Antoniou, A. 2015. "Ncorr: Open-Source 2D Digital Image Correlation Matlab Software." *Experimental Mechanics*, 55 (6), 1105–1122. https://doi.org/10.1007/s11340-015-0009-1.

Carril, J. L., LaBoube, R. A., and Yu, W. 1994. *Tensile and bearing capacities of bolted connections*. First Summary Report, Civil Engineering Study 94-1, University of Missouri-Rolla, Rolla, Missouri, 185.

Chong, K. P., and Matlock, R. B. 1975. “Light-gage steel bolted connections without washers.” *Journal of the Structural Division*, 101 (7) : 1381–1391.

ECS. 2006. *Eurocode 3. Design of steel structures, Part 1.3 General rules - Supplementary rules for cold formed thin gauge members and sheeting*. EN-1993-1-3: 2006, European Committee for Standardisation, Brussels, Belgium.

Fox, D. M., and Schuster, R. M. 2006. “Single Bolted Tension Member Design - a New Approach.” *Proceedings of the Eighteenth International Specialty Conference on Cold-Formed Steel Structures*, University of Missouri, Rolla, MO, 21.

He, Y. C., and Wang, Y. C. 2011. “Load–deflection behaviour of thin-walled plates with a single bolt in shearing.” *Thin-Walled Structures*, 49 (10), 1261–1276. https://doi.org/10.1016/j.tws.2011.05.008.

Kulak, G. L., and Grondin, G. Y. 2001. “AISC LRFD rules for block shear in bolted connections- A review.” *Engineering Journal*, 38 (4), 199–203.

Meimand, V. Z., and Schafer, B. W. 2014. “Impact of load combinations on structural reliability determined from testing cold-formed steel components.” *Structural Safety*, 48, 25–32. https://doi.org/10.1016/j.strusafe.2013.10.006.

Rogers, C. A., and Hancock, G. J. 1998. “Bolted connection tests of thin G550 and G300 sheet steels.” *Journal of Structural Engineering*, 124 (7) : 798–808. https://doi.org/10.1061/(ASCE)0733-9445(1998)124:7(798).

Rogers, C. A., and Hancock, G. J. 2000. “Failure Modes of Bolted-Sheet-Steel Connections Loaded in Shear.” *Journal of Structural Engineering*, 126 (3) : 288–296. https://doi.org/10.1061/(ASCE)0733-9445(2000)126:3(288).

Schijve, J. 2009. *Fatigue of structures and materials*. Springer, Dordrecht.

Soo Kim, T., and Kuwamura, H. 2007. "Finite element modeling of bolted connections in thin-walled stainless steel plates under static shear." *Thin-Walled Structures*, 45 (4), 407–421. https://doi.org/10.1016/j.tws.2007.03.006.

Teh, L. H., and Uz, M. E. 2015. "Ultimate Shear-Out Capacities of Structural-Steel Bolted Connections." *Journal of Structural Engineering*, 141 (6) : 04014152. https://doi.org/10.1061/(ASCE)ST.1943-541X.0001105.

Teh, L. H., and Uz, M. E. 2017. "Ultimate Tilt-Bearing Capacity of Bolted Connections in Cold-Reduced Steel Sheets." *Journal of Structural Engineering*, 143 (4) : 04016206. https://doi.org/10.1061/(ASCE)ST.1943-541X.0001702.

Winter, G. 1956. *Light gage steel connections with high-strength, high-torqued bolts*. Center for Cold-Formed Steel Structures Library, 513–528.

Xing, H., Teh, L. H., Jiang, Z., and Ahmed, A. 2020. "Shear-Out Capacity of Bolted Connections in Cold-Reduced Steel Sheets." *Journal of Structural Engineering*, 146 (4) : 04020018. https://doi.org/10.1061/(ASCE)ST.1943-541X.0002565.

Yu, W. 1982. "AISI Design Criteria for Bolted Connections." *Proceedings of the Sixth International Specialty Conference on Cold-Formed Steel Structures*, University of Missouri, Rolla, MO, 675–698.

Zadanfarrokh, F., and Bryan, E. R. 1992. "Testing and Design of Bolted Connections in Cold Formed Steel Sections." *Proceedings of the Eleventh International Specialty Conference on Cold-Formed Steel Structures*, University of Missouri, Rolla, MO, 625–666.

Appendix A

This appendix lists the design equation comparison each test specimen in Table A-1. The design equations considering tilting are only applied to single-lap connections.

Notation

A_{nv}	=	Area of shear plane (mm^2) [in^2]
C	=	Bearing factor
C_c	=	Correlation coefficient
C_P	=	Correction factor
C_ϕ	=	Calibration coefficient
d	=	Bolt diameter (mm) [in]
d_h	=	Bolt hole diameter (mm) [in]
e	=	End distance (mm) [in]
e_{net}	=	Net end distance (mm) [in]
F_m	=	Mean value of fabrication factor
F_u	=	Ultimate stress (MPa) [ksi]
F_{u2}	=	Ultimate stress of the sheet not in contact of screw head (MPa) [ksi]
F_y	=	Yield stress (MPa) [ksi]
k_t	=	Eurocode thickness modification factor
L_{av}	=	Active shear plane length (mm) [in]
M_m	=	Mean value of material factor
m_f	=	Connection type modification factor
P_m	=	Mean value of professional factor
P_n	=	Nominal strength (kN) [kip]
P_u	=	Ultimate load (kN) [kip]
$P_{u,s}$	=	Ultimate load of single-lap joint (kN) [kip]
$P_{u,d}$	=	Ultimate load of double lap joint (kN) [kip]
t	=	Sheet thickness (mm) [in]
t_2	=	Thickness of the sheet not in contact of screw head (mm) [in]
V_M	=	Coefficient of variation of material factor
V_F	=	Coefficient of variation of fabrication factor
V_P	=	Coefficient of variation of test results
V_Q	=	Coefficient of variation of load effect
W_{net}	=	Sheet net width (mm) [in]
ϕ	=	Resistance factor (LRFD)
Ω	=	Safety factor (ASD)
α_b	=	Eurocode bearing/tearing modification factor
β_0	=	Target reliability index
ϵ_u	=	Strain at the ultimate tensile stress (MPa) [ksi]
σ_b	=	Bearing stress (MPa) [ksi]

Table 1. Summary of design equations for comparison

Equation number	Source	Format
Eq. (1)	AISI S100 E4.3.2 (2007)	$P_n = teF_u$
Eq. (2)	AISI S100 J6.1 (2016)	$P_n = 1.2te_{net}F_u$
Eq. (3)	Teh and Uz (2015)	$P_n = 1.2(e_{net} + d_h/4)tF_u$
Eq. (4)	Xing et al. (2020)	$P_n = 1.2(3d/e)^{1/5}(e_{net} + d_h/4)tF_u$
Eq. (5)	EN 1993-1-3 (2006)	$P_n = \begin{cases} (0.8t/3 + 0.5)teF_u & t \le 1.25 \text{ mm} \\ teF_u/1.2 & t > 1.25 \text{ mm} \end{cases}$
Eq. (6)	AISI S100 J4.3.1 (2016)	$P_n = 4.2(t_2^3 d)^{1/2}F_{u2}$
Eq. (7)	AISI S100 J3.3.1 (2016)	$P_n = Cm_f dtF_u$
Eq. (8)	Teh and Uz (2017)	$P_n = 2.65d^{1/2}t^{4/3}w_{net}^{1/6}F_u$

Table 2. Average material properties

	Longitudinal				Transverse			
Thickness, t mm (mil, ga.)	Mean F_y MPa (ksi)	Mean F_u MPa (ksi)	Mean ε_u	Quantity	Mean F_y MPa (ksi)	Mean F_u MPa (ksi)	Mean ε_u	Quantity
0.84 (33, 20)	328 (47.6)	397 (57.6)	0.223	3	370 (53.7)	390 (56.6)	0.168	2
1.37 (54, 16)	401 (58.1)	483 (70.1)	0.166	2	412 (59.8)	482 (69.9)	0.139	6
2.46 (97, 12)	353 (51.2)	472 (68.5)	0.176	3	350 (50.8)	485 (70.4)	0.141	2

Table 3. Comparison of ultimate load between single-lap (titling) and double-lap (non-tilting) connections

	Single-lap		Double-lap		Single/Double
Specimen	$P_{u,s}$, kN (kip)		$P_{u,d}$, kN (kip)		$P_{u,s}/P_{u,d}$
20g-3/8-1.75dh	4.98	(1.12)	5.27	(1.19)	0.944
16g-3/8-1.75dh	10.03	(2.26)	10.78	(2.42)	0.931
12g-3/8-1.75dh	17.46	(3.93)	21.84	(4.91)	0.800
20g-1/2-1.75dh	4.62	(1.04)	7.14	(1.60)	0.647
16g-1/2-1.75dh	10.41	(2.34)	14.31	(3.22)	0.728
12g-1/2-1.75dh	24.68*	(5.55)*	27.93*	(6.28)*	0.884
Mean					0.822
C.o.V.					0.145
20g-3/8-1.50dh	4.21	(0.95)	5.15	(1.16)	0.817
16g-3/8-1.50dh	9.12	(2.05)	9.08	(2.04)	1.003
12g-3/8-1.50dh	18.11*	(4.07)*	18.32	(4.12)	0.989
20g-1/2-1.50dh	4.91	(1.10)	6.38	(1.43)	0.770
16g-1/2-1.50dh	10.77	(2.42)	12.53*	(2.82)*	0.859
12g-1/2-1.50dh	22.91*	(5.15)*	25.42	(5.71)	0.901
Mean					0.890
C.o.V.					0.105
20g-3/8-1.25dh	3.70	(0.83)	4.13	(0.93)	0.896
16g-3/8-1.25dh	9.04	(2.03)	7.57	(1.70)	1.194
12g-3/8-1.25dh	15.56	(3.50)	15.24*	(3.43)*	1.021
20g-1/2-1.25dh	4.99	(1.12)	5.16	(1.16)	0.967
16g-1/2-1.25dh	11.39*	(2.56)*	10.13*	(2.28)*	1.125
12g-1/2-1.25dh	21.41	(4.81)	19.58	(4.40)	1.094
Mean					1.049
C.o.V.					0.104
Mean (all)					0.920
C.o.V. (all)					0.153

* Snug-tight bolt installation at the torque of 16.9 N-m (12.5 lbf-ft)

Table 4. Comparison of test-to-predicted ratios between design equations

			Single-lap			Double-lap		
Number	Design equation		P_u/P_n	ϕ	Ω	P_u/P_n	ϕ	Ω
Eq. (1)	AISI S100 E4.3.2 (2007)			0.55	2.93		0.77	2.08
		Mean	0.877			1.071		
		C.o.V.	0.163			0.072		
Eq. (2)	AISI S100 J6.1 (2016)			0.61	2.60		0.86	1.86
		Mean	1.118			1.339		
		C.o.V.	0.219			0.148		
Eq. (3)	Teh and Uz (2015)			0.53	3.04		0.75	2.12
		Mean	0.883			1.067		
		C.o.V.	0.184			0.087		
Eq. (4)	Xing et al. (2020)			0.49	3.26		0.69	2.32
		Mean	0.790			0.961		
		C.o.V.	0.165			0.071		
Eq. (5)	EN 1993-1-3 Table 8.4 (2006)			0.71	2.26		0.94	1.70
		Mean	1.090			1.295		
		C.o.V.	0.141			0.063		
Eq. (6)	AISI S100 J4.3.1 (2016)			0.55	2.90		n/a	n/a
		Mean	0.913			n/a		
		C.o.V.	0.177			-		
Eq. (7)	AISI S100 J3.3.1 (2016)			0.55	2.90		n/a	n/a
		Mean	0.791			n/a		
		C.o.V.	0.098			-		
Eq. (8)	Teh and Uz (2017)			0.57	2.80		n/a	n/a
		Mean	0.864			n/a		
		C.o.V.	0.131			-		
Eq. (9)	Recommended method (1)			0.68	2.34		n/a	n/a
	min(Eq. (1) and (5))	Mean	0.994			n/a		
		C.o.V.	0.108			-		
Eq. (10)	Recommended method (2)			0.68	2.37		n/a	n/a
	min(Eq. (3) and (5))	Mean	1.002			n/a		
		C.o.V.	0.119			-		

Note. Measured thickness, geometry, and material properties used in P_n predictions.

Table 5. Summary of test-to-predicted ratios of different datasets

	Quantity	Eq. (1)	Eq. (2)	Eq. (3)	Eq. (4)	Eq. (5)
This paper	18	0.96	1.21	0.96	0.86	1.20
Xing et al. (2020)	60	1.10	1.36	1.09	0.98	1.32
He and Wang (2011)	4	1.17	1.55	1.19	1.06	1.41

Table A-1. List of test-to-predicted ratio for all specimens

Specimen	Test-to-predicted ratio P_u/P_n									
	Eq. (1)	Eq. (2)	Eq. (3)	Eq. (4)	Eq. (5)	Eq. (6)	Eq. (7)	Eq. (8)	Eq. (9)	Eq. (10)
20g-3/8-1.75dh-S	0.824	0.957	0.799	0.746	1.105	1.221	0.951	1.102	1.221	1.221
16g-3/8-1.75dh-S	0.887	1.029	0.861	0.804	1.065	1.076	0.900	1.042	1.076	1.076
12g-3/8-1.75dh-S	0.832	0.982	0.813	0.753	0.998	0.698	0.809	0.749	0.832	0.813
20g-1/2-1.75dh-S	0.575	0.667	0.558	0.516	0.774	0.971	0.777	0.827	0.971	0.971
16g-1/2-1.75dh-S	0.655	0.764	0.637	0.588	0.786	0.855	0.653	0.791	0.855	0.855
12g-1/2-1.75dh-S	0.872	1.020	0.849	0.782	1.047	0.849	0.827	0.863	0.872	0.849
20g-3/8-1.50dh-S	0.813	1.014	0.812	0.734	1.089	1.026	0.799	0.927	1.026	1.026
16g-3/8-1.50dh-S	0.958	1.197	0.958	0.865	1.150	0.985	0.822	0.952	0.985	0.985
12g-3/8-1.50dh-S	0.935	1.161	0.933	0.844	1.122	0.688	0.811	0.743	0.935	0.933
20g-1/2-1.50dh-S	0.742	0.920	0.740	0.663	1.011	1.096	0.877	0.927	1.096	1.096
16g-1/2-1.50dh-S	0.806	1.001	0.804	0.720	0.967	0.925	0.710	0.851	0.925	0.925
12g-1/2-1.50dh-S	0.933	1.165	0.932	0.834	1.119	0.780	0.762	0.793	0.933	0.932
20g-3/8-1.25dh-S	0.826	1.133	0.856	0.748	1.098	0.871	0.676	0.789	0.871	0.871
16g-3/8-1.25dh-S	1.169	1.621	1.217	1.060	1.403	1.018	0.837	0.980	1.169	1.217
12g-3/8-1.25dh-S	1.004	1.385	1.043	0.910	1.205	0.628	0.725	0.672	1.004	1.043
20g-1/2-1.25dh-S	0.868	1.201	0.903	0.779	1.165	1.033	0.826	0.881	1.033	1.033
16g-1/2-1.25dh-S	1.043	1.449	1.087	0.937	1.252	0.989	0.760	0.909	1.043	1.087
12g-1/2-1.25dh-S	1.052	1.460	1.095	0.944	1.262	0.734	0.716	0.746	1.052	1.095
20g-3/8-1.75dh-ID	0.890	1.038	0.865	0.806	1.200	n/a	n/a	n/a	n/a	n/a
16g-3/8-1.75dh-ID	0.948	1.100	0.919	0.858	1.137	-	-	-	-	-
12g-3/8-1.75dh-ID	1.034	1.204	1.005	0.936	1.241	-	-	-	-	-
20g-1/2-1.75dh-ID	0.935	1.086	0.908	0.839	1.278	-	-	-	-	-
16g-1/2-1.75dh-ID	0.942	1.107	0.919	0.844	1.131	-	-	-	-	-
12g-1/2-1.75dh-ID	0.988	1.155	0.962	0.886	1.186	-	-	-	-	-
20g-3/8-1.50dh-ID	1.044	1.308	1.045	0.943	1.416	-	-	-	-	-
16g-3/8-1.50dh-ID	0.988	1.247	0.992	0.893	1.186	-	-	-	-	-
12g-3/8-1.50dh-ID	0.989	1.227	0.986	0.893	1.187	-	-	-	-	-
20g-1/2-1.50dh-ID	0.893	1.111	0.891	0.798	1.184	-	-	-	-	-
16g-1/2-1.50dh-ID	0.905	1.131	0.905	0.810	1.087	-	-	-	-	-
12g-1/2-1.50dh-ID	1.041	1.297	1.040	0.931	1.249	-	-	-	-	-
20g-3/8-1.25dh-ID	0.959	1.309	0.993	0.869	1.296	-	-	-	-	-
16g-3/8-1.25dh-ID	0.917	1.250	0.949	0.831	1.101	-	-	-	-	-
12g-3/8-1.25dh-ID	0.993	1.357	1.028	0.899	1.191	-	-	-	-	-
20g-1/2-1.25dh-ID	0.854	1.173	0.886	0.766	1.130	-	-	-	-	-
16g-1/2-1.25dh-ID	0.958	1.365	1.007	0.862	1.149	-	-	-	-	-
12g-1/2-1.25dh-ID	0.968	1.344	1.008	0.869	1.162	-	-	-	-	-

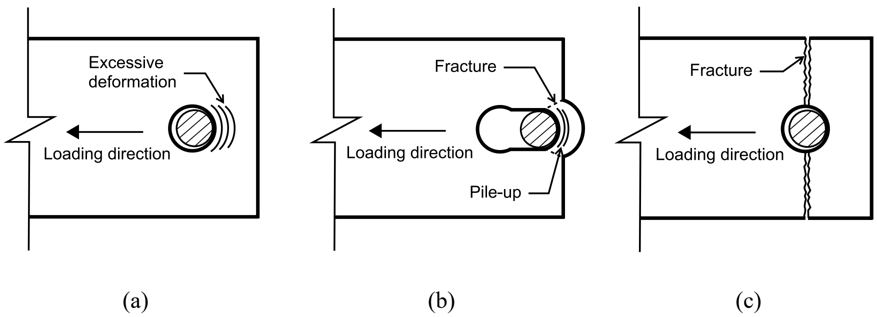

Fig. 1. Failure modes of connected plates (a) bearing failure (b) end tear-out failure (c) net section fracture failure

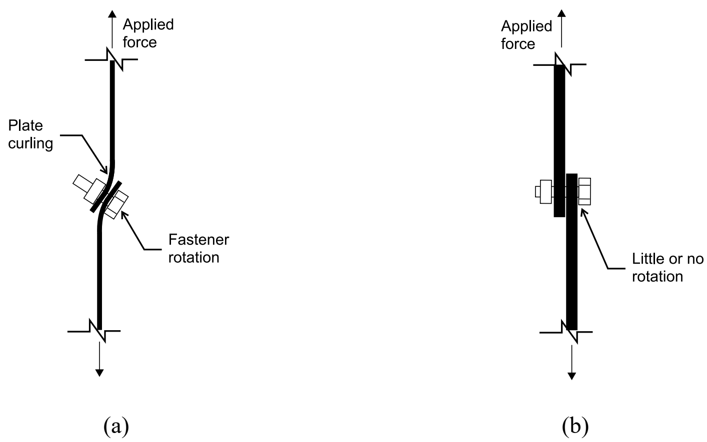

Fig. 2. Schematic deformation of thin-plate and thick-plate single-lap shear connections with single bolt (a) tilting in a thin plates (b) and little to no tilting in thick plates

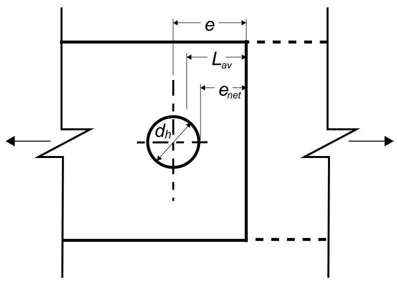

Fig. 3. Example dimensions of a single-lap shear bolted connection

Formatted: Font: Not Bold

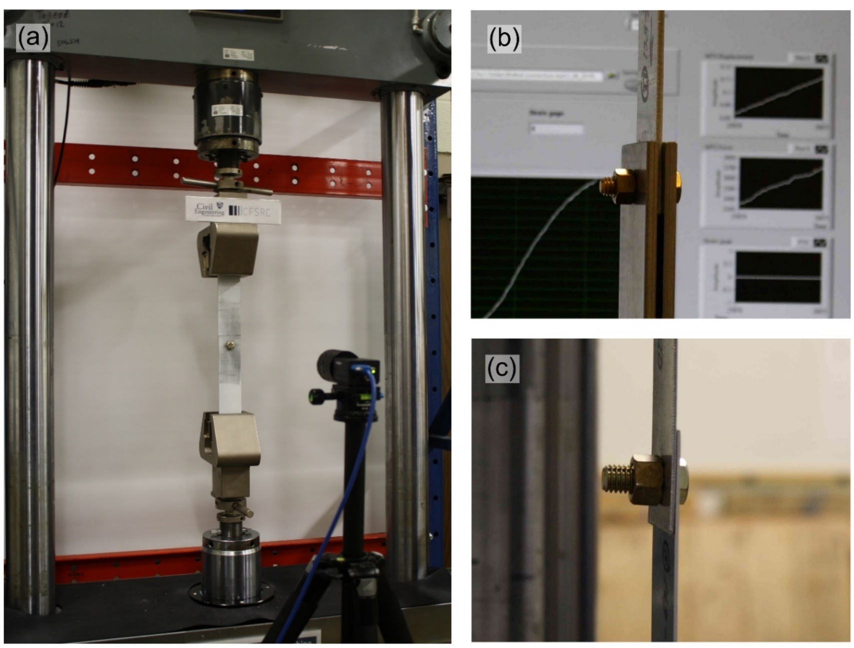

Fig. 4. Test set-up (a) MTS loading machine (b) double-lap connection (c) single-lap connection

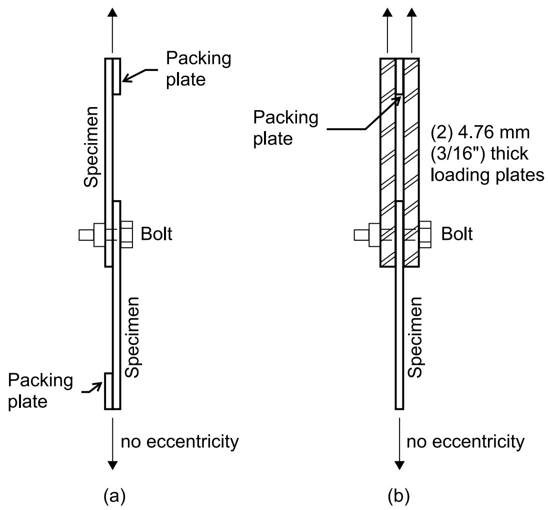

Fig. 5. Schematic view of testing (a) single-lap connection (b) double-lap connection

6

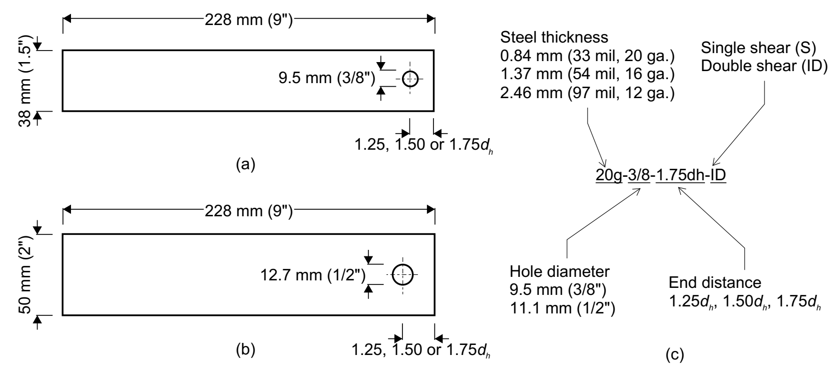

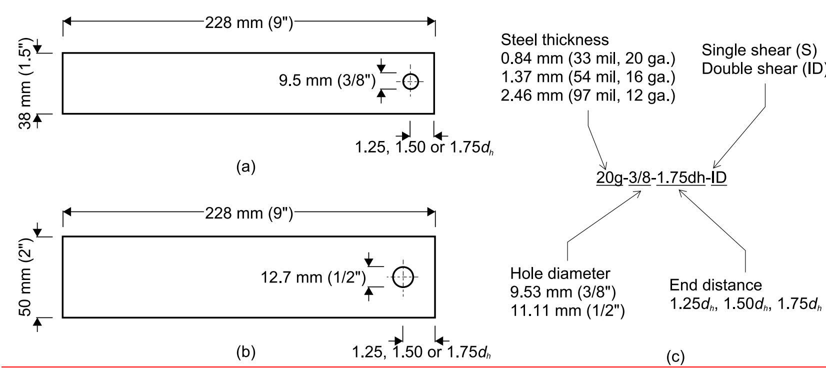

Fig. 6. Schematic view of specimen (a) specimen for 9.5 mm (3/8 in.) hole diameter (b) specimen for 12.7 mm (1/2 in.) hole diameter (c) specimen designation

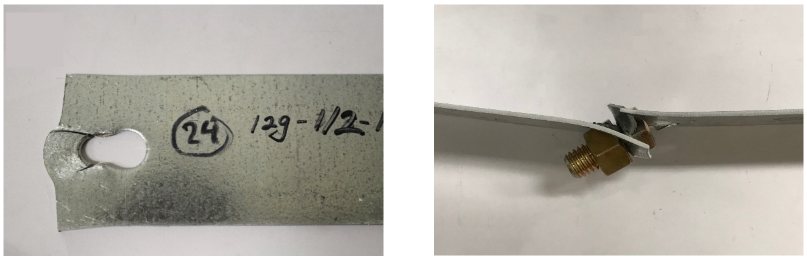

(a) (b)

Fig. 7. Failure forms (a) double-lap (b) single-lap

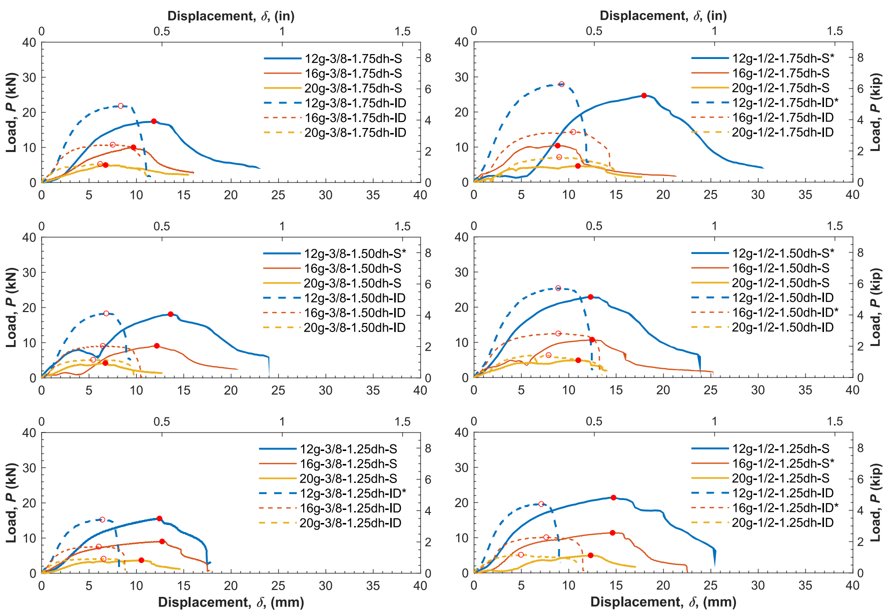

* Snug-tight bolt installation at the torque of 16.9 N-m (12.5 lbf-ft)

~~* Snug-tight bolt installation at the torque of 16.9 N-m (12.5 lbf-ft)~~

Fig. 8. Load deformation curves of single-lap and double-lap connections

Formatted: Font: (Default) Times New Roman

Formatted: Font: (Default) Times New Roman, 11 pt

Formatted: Font: (Default) Times New Roman

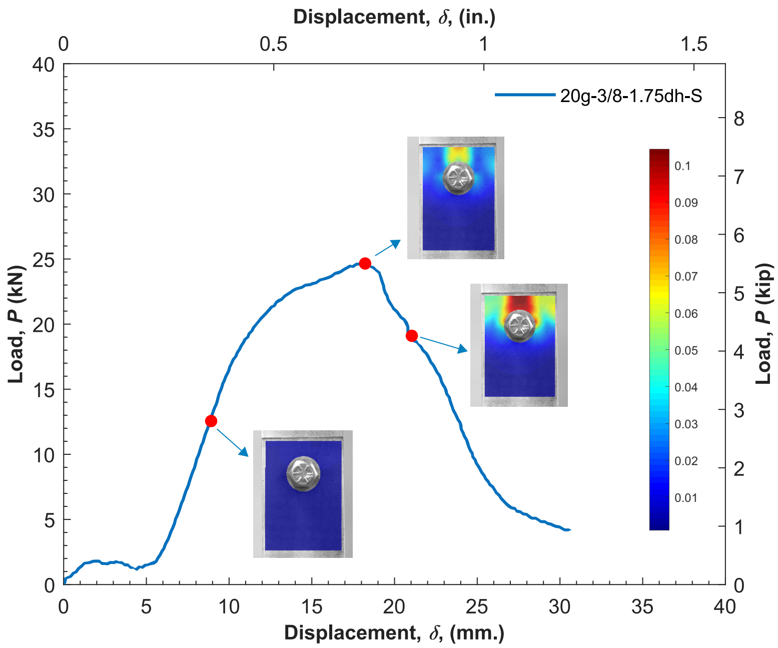

Fig. 9. Connection equivalent von Mises strain evolution over the load-deformation history

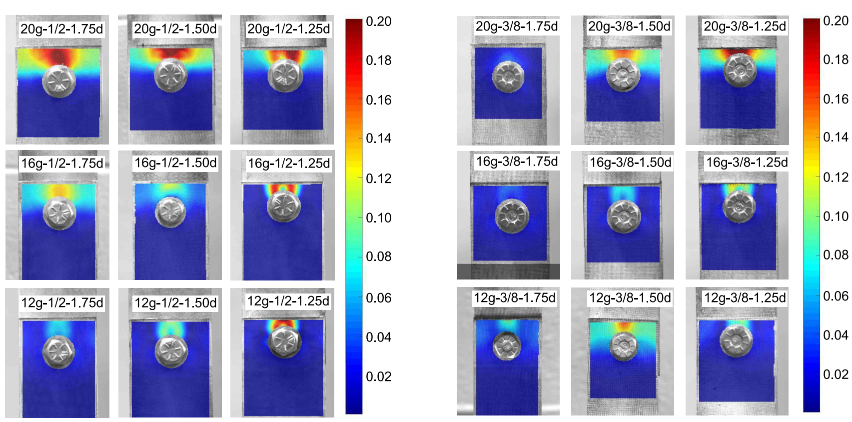

(a) (b)

Fig. 10. Connection responses at peak load (a) DIC strain contours of 1/2 in. hole diameter series specimens (b) DIC strain contours of 3/8 in. hole diameter series specimens

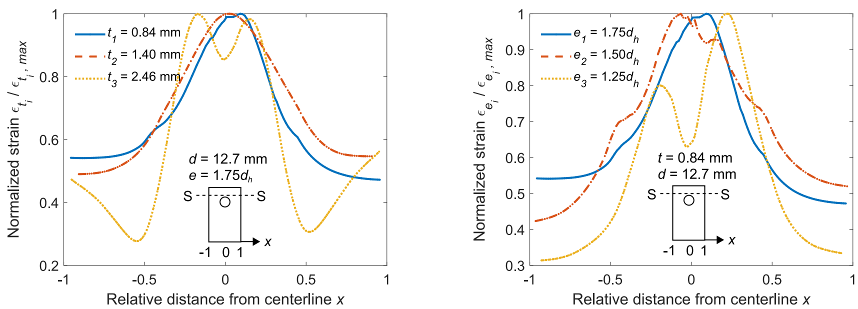

(a) (b)

Fig. 11. Strain distributions near bolt hole (a) varying thickness (b) varying end distance

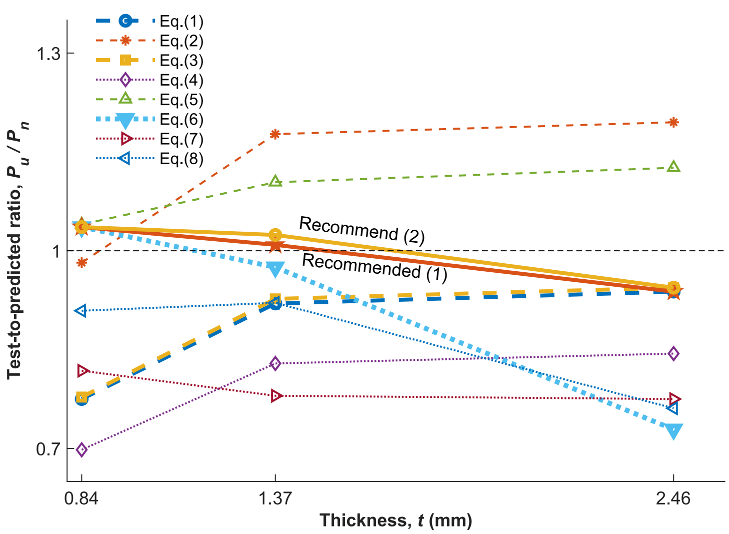

Fig. 12. Test-to-predicted ratio versus sheet thickness for single-lap connections

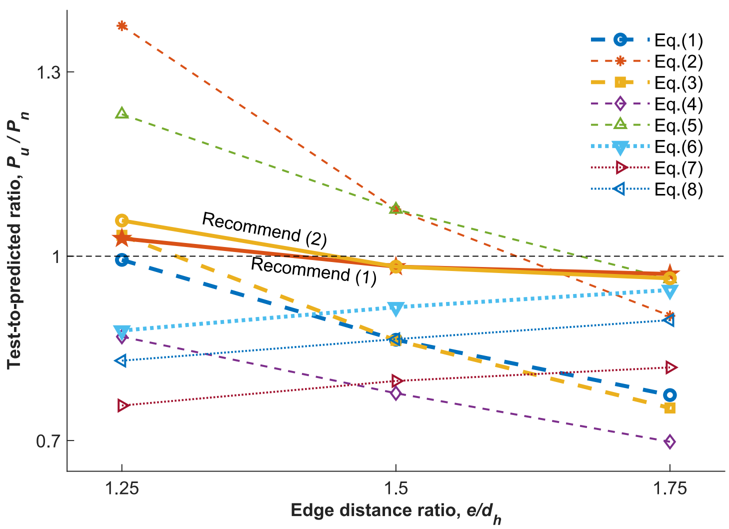

Fig. 13. Test-to-predicted ratio versus end distance ratio for single-lap connections